Intelligent Secondary Control of Islanded AC Microgrids: A Brain Emotional Learning-based Approach

Yeganeh, Mohammad Sadegh Orfi; Oshnoei, Arman; Mijatovic, Nenad; Dragicevic, Tomislav; Blaabjerg, Frede

Published in:
IEEE Transactions on Industrial Electronics

Link to article, DOI:
10.1109/TIE.2022.3203677

Publication date:
2023

Document Version
Peer reviewed version

Intelligent Secondary Control of Islanded AC Microgrids: A Brain Emotional Learning-based Approach

Mohammad Sadegh Orfi Yeganeh, *Member, IEEE*, Arman Oshnoei, *Member, IEEE*, Nenad Mijatovic, *Senior Member, IEEE*, Tomislav Dragicevic, *Senior Member, IEEE*, and Frede Blaabjerg, *Fellow, IEEE*

***Abstract*—This paper proposes a distributed intelligent secondary control (SC) approach based on brain emotional learning-based intelligent controller (BELBIC) for power electronic-based ac microgrid (MG). The BELBIC controller is able to learn quick-auto and handle model complexity, nonlinearity, and uncertainty of the MG. The proposed controller is fully model-free, indicating that the voltage amplitude and frequency deviations are regulated without previous knowledge of the system model and parameters. This approach ensures low steady-state variations with higher bandwidth and maintains accurate power-sharing of the droop mechanism. Furthermore, primary control is realized with a robust finite control set-model predictive control (FCS-MPC) in the inner level to increase the system frequency bandwidth and a droop control in the outer level to regulate the power-sharing among the distributed generations. Finally, experimental tests obtained from a hardware-in-the-loop testbed validate the proposed control strategy for different cases.**

***Index Terms*—Brain emotional learning based intelligent controller (BELBIC), Distributed generation (DG), Finite control set model predictive control (FCS-MPC), Microgrid (MG), Voltage source converter (VSC).**

I. Introduction

ISLANDED microgrids (MGs) are a group of interconnected loads and distributed generations (DGs), and they are usually interfaced to the grid through power converters to reduce pollution and power transmission losses, and obtain high-energy utilization rates with the flexibility of different installation locations [1]. The most significant challenges in islanded AC MGs are finding solutions for optimal power flow, increasing systems reliability and robustness, improving the stability characteristics of voltage and frequency, and power-angle in dynamic loads, constant loads, and inductor motor [2], [3]. To ensure the control of MG dynamics, a hierarchical control structure including primary control (PC), secondary control (SC), and tertiary control (TC) is defined [4]–[6]. The PC stabilizes the voltage and frequency and offers power-sharing capability among DGs. The SC can restore the voltage and frequency deviations created by PC operations. The TC handles the power flow management between the grid and MGs at the Point of Common Coupling (PCC).

In the PC layer, the reactive power-voltage amplitude (Q-E) and real power-frequency (P-ω) droop control method has been implemented to ensure the advantages of being communication-free for the power-sharing mechanism, and voltage and frequency stability [7], [8]. The main challenge of the droop control is steady-state errors, which the SC section is considered to compensate for this drawback. Besides, another restriction is communication network time delay and the bandwidth (BW) of the PC that many controllers have been used to improve this shortage, which is originated from the low-speed range of multiplying modules and instruments [9]–[15]. Conventional controllers such as proportional-integral (PI) and proportional resonant controllers have simple concepts and functionality and are easy to implement but they suffer from unbalancing in steady-state and transient performance and have reduced performance while the output frequency changes. To make an improvement on the BW and mentioned drawbacks, finite control set-model predictive control (FCS-MPC) has been replaced by a cascaded multi-loop structure [10]. This controller is recognized as one of the most promising controllers for industry and power electronic applications such as power converter/motor drives due to its capability over real-time solutions (one-step-ahead prediction) with multiple objectives and constraints [16], [17].

SC schemes can be categorized into centralized, distributed, and decentralized schemes [18]. Under a centralized SC strategy, an MG controller gathers data from the PCC and restores voltage and frequency by a PI controller. The controller output signal is then sent to local controllers of each DG through communication links. The centralized methods can attain suitable voltage and frequency restoration. However, reliance on the MG controller and one-to-all communication structure decreases system reliability as the breakdown of the MG controller or communication can collapse the entire MG. To realize the SC based on local variables of the DGs, decentralized approaches have been proposed. However, these methods require a thorough knowledge of the MG topology to evaluate the variables [18]–[21]. In light of reliability, distributed SC schemes separated from MG central controller can be considered as a tradeoff between the centralized and decentralized schemes [22]–[25]. In [26], a distributed SC for voltage variations via feedback linearization is introduced. However, the method entirely depends on MG parameters. A general SC structure based on the distributed averaging PI is proposed in [27]. Nevertheless, the low bandwidth SC was utilized to compensate for voltage and frequency deviations, making the MG very slow. A secondary controller consisting of a PI regulator for voltage and frequency restoration has been presented in [12], [28]. However, PI-based SC risks switching failure and deteriorates real power-sharing. In [17], [29], a fuzzy controller is used in the SC level to damp the voltage and frequency deviations with higher bandwidth. However, the system performance is impacted by the fixed fuzzy rules employed in the design procedure of the controller. A finite-time secondary control method is presented in [30], [31] to perform precise reactive power sharing and regulate the frequency and voltage of an islanded MGs. However, the upper bound of the finite convergence time relies on the MG's initial condition before triggering the control methods. Thus, finite-time control strategies can not guarantee a specified convergence since priori initial operation conditions are usually unavailable. In order to reach higher compatibility

and reliability, battery systems are involved within islanded MGs. Utilizing distributed secondary control for energy storage systems is discussed in [32], where a distributed terminal sliding mode controller is used to execute active power sharing and match the state of charge of the distributed energy storage systems. In [33], a distributed sliding mode controller is proposed for voltage and frequency restoration and accurate active power-sharing in an islanded MG. However, these controllers do not consider reactive power sharing. As a consequence, the secondary control methods reported in the previous studies mainly rely on the operating point conditions, which makes them less robust and reliable. Although some researchers have developed online tuning approaches to avoid this dependency [11], they still demand a precise mathematical instance, which is a complex and time-consuming duty. Moreover, the changing conditions and variations of the MG imply that there is no fixed mathematical model for all system conditions. In such a design, model mismatches or unexpected changes in the MG's configuration or parameters affect the controller's performance, particularly in steady-state.

The intelligent approaches rehabilitate such shortcomings in obtaining a robust performance in various operating conditions of MGs. The main characteristic of intelligent approaches is the model-free structure that enables them to handle model complexity, non-linearity, and uncertainty in power electronic applications. The brain emotional learning-based intelligent controller (BELBIC) is a model-free intelligent controller with a simplistic control framework [34], [35], making it viable for practical applications in real-time. This method has a reinforcement learning process as a principle, effectively tackling disturbances and uncertainties in the system. However, unlike the reinforcement learning methods in the machine learning area, BELBIC does not present the need for exhaustive training [36]. Minimal computational intricacy, online learning ability, and no requirement for prior knowledge of MG dynamics make BELBIC a unique controller over other intelligent controllers such as artificial neural network (ANN) and fuzzy logic control. Also, it is simple, with rarer tuning parameters in emotional regulators, and, unlike ANNs, it does not demand an extra iterative procedure for learning or correcting parameters. In contrast, in neural network control, the network topology, like the number of nodes, layers, and parameters in the activation functions, are essential considerations that must be appropriately considered [37]. In [38], the BELBIC controller has superior performance compared with PI and fuzzy logic controllers in both online and offline simulations for PMSM drive systems in different test conditions. It is shown in [39] that the BELBIC can offer more effective solutions than fuzzy logic and neural network in controlling the synchronous machines in power systems.

Motivated by the previous discussions, this paper proposes a model-free and adaptive controller based on BELBIC to provide accurate voltage and frequency compensator signals for VSC-based islanded ac MG. In this way, neither the parameters nor structures of the system are needed beforehand. Unlike the conventional controllers generally designed for fixed operating conditions, the BELBIC avoids the dependency of the control system on the operating conditions and demonstrates robust performance in load disturbances and uncertainties. A mathematical representation is also provided to evaluate the convergence conditions of the controller. The control scheme performance is compared to a ANN-PI controller and a control strategy reported in [12]. The proposed control scheme compensates for the steady-state voltage and frequency deviations using an entirely distributed procedure and preserves active and reactive power sharing during both steady state and transitions. An FCS-MPC method is initially presented in the inner level of the PC section to control the voltage of VSCs. The VSCs' voltage regulation is improved with a fast transient response by employing FCS-MPC. Simulation and experimental validations are provided to demonstrate the effectiveness of the proposed control strategy.

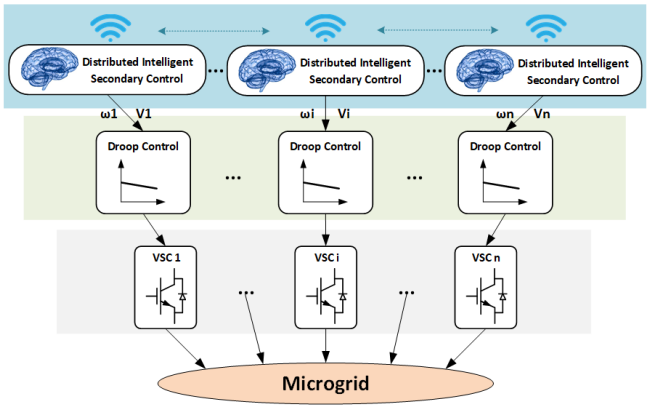

Fig. 1: General view of an islanded AC microgrid.

II. Principles of AC Microgrid Control

Fig.1 demonstrates the communication layer and distributed intelligent SC section between AC and DC sources like wind energy and photovoltaic systems. Distributed control is one of the most desired communication-based control techniques that does not need a central controller. Therefore, the information is only for each unit and requires a lower bandwidth [3]. Then, the SC layer sends ω and v references to the droop section to realize the voltage and frequency regulation. The droop section should adjust the power-sharing (active and reactive) among DGs to provide a balance inside the MG. Besides, a robust FCS-MPC has been utilized in the inner controller.

A. Power Calculation and Droop Sections

The droop control is employed to control active and reactive power-sharing and synchronize each converter. The droop control mechanism can be expressed as

$$\omega_{ref} = \omega_{n_i} - D_{P_i}.P_i \tag{1}$$

$$v_{ref} = v_{n_i} - D_{Q_i}.Q_i \tag{2}$$

where ω_{ref} and v_{ref} are the reference frequency and voltage respectively; ω_{n_i} and v_{n_i} are the nominal frequency and voltage of each DG unit, respectively; D_{P_i} and D_{Q_i} are the droop coefficients, which are chosen based on the rated power of the DG unit and the permissible deviations in frequency and voltage amplitude; and P_i and Q_i are the filtered active and reactive powers of DG_i, as follows:

$$P_i = G_L p_i \qquad p_i = v_{o\alpha i} i_{o\alpha i} + v_{o\beta i} i_{o\beta i} \tag{3}$$

$$Q_i = G_L q_i \qquad q_i = v_{o\beta i} i_{o\alpha i} + v_{o\alpha i} i_{o\beta i} \tag{4}$$

where $G_L = \frac{\omega_c}{\omega_c + s}$ denotes a low-pass filter with cutoff frequency ω_c; P_i and Q_i are the measured active and reactive powers of DG_i; and v_o and i_o are the instantaneous output voltage and current of DG_i in α-β frame.

B. Primary Control

There are three cascaded control sections in converters' conventional current-regulation-based inner controller to ensure voltage and frequency stability. Voltage control loop, current control loop, and modulation section (PWM). An alternative robust FCS-MPC controller is proposed in the PC section, in order to improve the dynamic performance of the integrated DGs. Based on [10], FCS-MPC controller can eliminate the series effect of low bandwidth from voltage and current control loops. Therefore, more BW flexibility and fast control response can be obtained by replacing a single FCS-MPC with a cascaded multi-loop structure, and achieving a BW improvement in the secondary section. The approximated BW of FCS-MPC is a few times more than the voltage and current control loops. FCS-MPC works based on calculating the cost function for all possible switching states on the three-phase VSC and then obtaining the desired v_i that minimizes the cost function. Fig. 2 illustrates eight possible switching states, voltage vectors, and related cost functions, in which a specific cost function can be obtained for each voltage vector. The value of CF_0 and CF_7 are the same but the difference is their effects on the switching orders (number of on and off switches at each cycle) and finally the value of switching losses. The output current (i_o), filter output current (i_f), and filter voltage (v_f) are presented in vectors as follows:

$$i_o = [i_{ou}\ \ i_{ov}\ \ i_{ow}]^T,\ i_f = [i_{fu}\ \ i_{fv}\ \ i_{fw}]^T,\ v_f = [v_{fu}\ \ v_{fv}\ \ v_{fw}]^T \tag{5}$$

Three-phase variable vectors are transferred to the two-dimensional vector ($\alpha\beta$ stationary reference frame) by employing the Clarke transformation (T) as $T = \frac{1}{3}[1\ \ e^{j\frac{2}{3}\pi}\ \ e^{j\frac{4}{3}\pi}]^T$. Finally, the output voltage and current of the converter can be expressed in the state-space form as follows:

$$\frac{d}{dt}\begin{bmatrix} i_f \\ v_f \end{bmatrix} = A\begin{bmatrix} i_f \\ v_f \end{bmatrix} + B\begin{bmatrix} v_i \\ i_o \end{bmatrix} \tag{6}$$

where

$$A = \begin{bmatrix} -\frac{R_f}{L_f} & -\frac{1}{L_f} \\ \frac{1}{C_f} & 0 \end{bmatrix},\quad B = \begin{bmatrix} \frac{1}{L_f} & 0 \\ 0 & -\frac{1}{C_f} \end{bmatrix} \tag{7}$$

Model predictive control technique works based on predicting v_f and i_f, and then applying the proper magnitude for V_{ref} in the objective function. In [13], a new strategy is proposed to improve the performance of the DC-link voltage quality of the VSC than the conventional FCS-MPC. Therefore, by tracking the voltage reference and its derivative simultaneously, the proposed strategy could improve the THD of the DC-link.

$$v_{ref}(k) = V_{ref}(cos(w_{ref}k) + jsin(w_{ref}k)) \tag{8}$$

$$v_{ref\alpha}(k) = V_{ref}cos(w_{ref}k) \tag{9}$$

$$v_{ref\beta}(k) = V_{ref}jsin(w_{ref}k) \tag{10}$$

where k is a representative for time, v_{ref} and w_{ref} are the voltage and frequency of the reference signals, respectively. By taking a time derivative of (8), the voltage derivative reference can be obtained:

$$\frac{dv_{ref}(k)}{dk} = w_{ref}V_{ref}cos(w_{ref}k) - jw_{ref}V_{ref}sin(w_{ref}k) \tag{11}$$

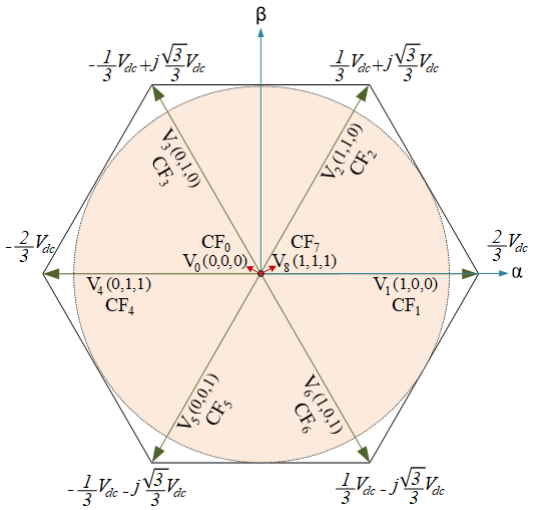

Fig. 2: Voltage vectors and switching states of a two-level three phase VSC.

In addition to tracking reference voltage by (8), $\frac{dv_f(k)}{dk}$ could also track $\frac{dv_{ref}(k)}{dk}$ to get better THD on the DC-link voltage. In order to form capacitor voltage derivative, predicted current i_f and measured current i_o are required:

$$\frac{dv_f(k)}{dt} = \frac{i_{f\alpha}(k) - i_{o\alpha}(k)}{C_f} + j\frac{i_{f\beta}(k) - i_{o\beta}(k)}{C_f} \tag{12}$$

It is intelligible that the voltage derivative can be well-tracked by minimizing the difference between the first and second terms of (11) and (12) as follows:

$$\begin{aligned} v_{reg}(k) = (C_f.w_{ref}.v_{ref\beta} - i_{f\alpha} + i_{o\alpha})^2 + \\ (C_f.w_{ref}.v_{ref\alpha} + i_{f\beta} - i_{o\beta})^2 \end{aligned} \tag{13}$$

Therefore, the main objective function consists of the prediction error (v_e) with a weighting factor (δ_1), the current limitation (ξ_{lim}), the number of switching efforts (SW) with a weighting factor (δ_2), and the minimizer for the voltage derivative (v_{reg}), which are as below:

$$v_e(k) = v_f(k+1) - v_{ref}(k) \tag{14}$$

$$\xi_{lim}(k) = \begin{cases} 0, & \text{if } \left| i_f(k) \right| \leq i_{max} \\ \infty, & \text{if } \left| i_f(k) \right| > i_{max} \end{cases} \tag{15}$$

$$SW(k) = \sum \left| u(k) - u(k-1) \right| \tag{16}$$

$$CF : \delta_1.v_e(k) + \xi_{lim}(k) + \delta_2.SW(k) + v_{reg}(k) \tag{17}$$

In addition, the weighting factors δ_1 and δ_2 can be determined by utilizing tools such as artificial neural network. In this study, these weighting factors are considered fixed values equal to 3 and 2, respectively.

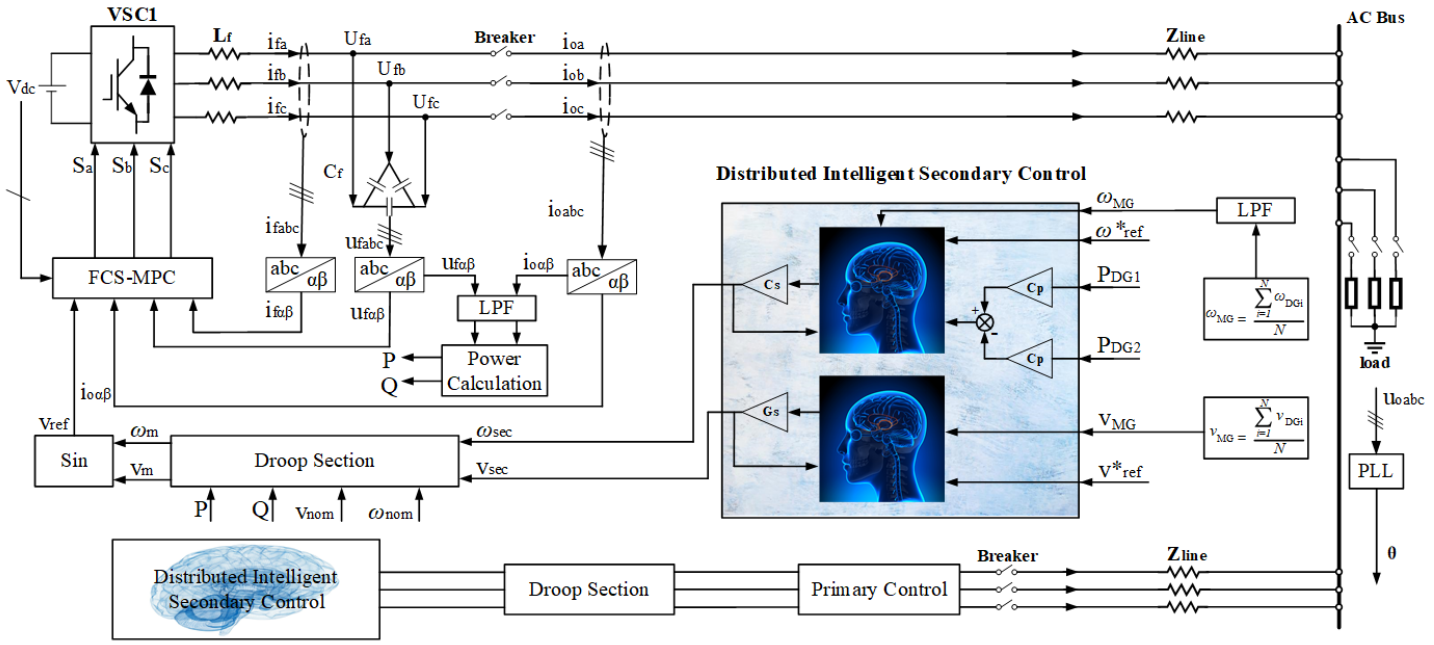

Fig. 3: Proposed scheme of the primary (FCS-MPC) and distributed secondary control of the VSC-based microgrid.

C. Secondary Control

The main duty of the SC is to compensate for the voltage amplitude and frequency deviations by sending the data to the PC. The SC section can regulate the voltage amplitude and frequency variations driven by PC. Mathematically, the SC section meets the following expressions:

$$\lim_{t \to t_c} \omega_i(t) = \omega_{ref} \tag{18}$$

$$\lim_{t \to t_c} v_i(t) = v_{ref} \tag{19}$$

As (5) and (6) imply, the frequency and voltage amplitude can be regulated in a finite time t_c. To share the active and reactive powers properly and (5) and (6) satisfactory, the correction terms are added to SC as follows:

$$\omega_{ref} = \omega_{n_i} - D_{P_i}.P_i + \delta_{\omega_{sec}} \tag{20}$$

$$v_{ref} = v_{n_i} - D_{Q_i}.Q_i + \delta_{v_{sec}} \tag{21}$$

where $\delta_{\omega_{sec}}$ and $\delta_{v_{sec}}$ are the frequency and voltage compensator signals provided by the SC, respectively. In this study, the SC is equipped with BELBIC to generate the control signals. A comprehensive investigation has been done on the SC in section IV.

III. Design of Intelligent Secondary Controller

Regulating voltage and frequency in the SC loop is one of the critical challenges for power converters in islanded AC MGs. In this study, the BELBIC is employed to recover the voltage and frequency magnitude to their nominal values and maintain the power-sharing among the DGs. More details over inputs and outputs of primary control, droop section, and secondary section are illustrated in Fig. 3. The controller comprises the Amygdala, which is in charge of emotional learning, the Orbitofrontal cortex, sensory cortex, and the Thalamus [35], [38]. The model has two inputs, including sensory input (SI) and emotional signal (ES). The sensory cortex receives the Thalamus output and then submits it to the Amygdala (A) and Orbitofrontal (O) cortex. Preprocessing on SI signal such as filtering or noise reduction is performed by the Thalamus. A and O networks, respectively, represent the functional blocks of the amygdala and orbitofrontal cortex. The subtraction of network A and network O outputs yields the BELBIC output, which is expressed by

$$u(t) = A(t) - O(t). \tag{22}$$

Network A is provided with the inputs of SI and ES. The SI input is multiplied by a predetermined connection weight (G) to obtain the output of network A, given by:

$$A(t) = SI(t)G(t) \tag{23}$$

where $G(t)$ changes in accordance with the following integral equation

$$G(t) = \int_0^t \delta g(t)dt + G(0) \tag{24}$$

where

$$\delta g(t) = \alpha SI(t)[max(0, ES(t) - A(t) - A_a(t)) \tag{25}$$

$$A_a(t) = max[SI(t)]G_a(t) \tag{26}$$

where α is the learning rate; A_a is a neuron that receives maximum sensory signals from the thalamus directly; $max[SI]$ is the maximum of all sensory signals. The dynamics of G_a is expressed by

$$G_a = \int_0^t \delta g_a dt + G_a(0). \tag{27}$$

The network O is provided with SI and ES inputs as well as the last model output. The network O output is computed by multiplying connection weight (H) into the SI signal.

$$O(t) = SI(t)H(t) \tag{28}$$

where $H(t)$ varies as follows:

$$H(t) = \int_0^t \delta h(t)dt + H(0) \tag{29}$$

where

$$\delta h(t) = \beta SI(t)[A(t) - O(t) - ES(t)] \tag{30}$$

where β represents the inhibition rate; taking the initial states $G(0) = H(0) = G_a(0) = 0$ into consideration, the BELBIC output in (22) can be written as

$$u(t) = SI(t)[\alpha \int_0^t SI(t)[max(0, ES(t) - A(t) - A_a(t))]dt - \beta \int_0^t SI(t)[A(t) - O(t) - ES(t)]dt]. \tag{31}$$

The A and O networks learning happens via its internal rules for adaptive weight update given by Eqs. (25) and (30). Updating the adaptive weights in the O network is similar to the A network rule, whereas its weight may decrease or increase as essential to follow the required inhibition.

Taking the computational model and execution characteristics of BELBIC on the SC into consideration, extracting the conditions that provide the BELBIC internal stability is required. The internal stability of BELBIC depends on the conditions for asymptotic convergence of the outputs of A and O networks. The convergence conditions will be discussed in the following section.

A. Convergence condition

Theorem 1. *Given the network weight adjustments as in (22) to (30), there exists a combination of SI signal, and parameters of α and β such that* [35]

$$1)|1 - \alpha SI(t)^2| < 1$$
$$2)|1 - \beta SI(t)^2| < 1$$

which confirms the convergence of the weights of network A and network O asymptotically.

Proof. The controller's behavior can be split into two distinct phases: transient and steady-state phases. Initially, during the transient phase, (25) can be expressed as:

$$\delta g(t) = \alpha SI(t)[ES(t) - A(t) - A_a(t)] \tag{32}$$

During the steady-state phase, the variation of weights of A and O networks is zero. i.e.

$$\delta g(t) = \delta g_a(t) = \delta h(t) = 0 \tag{33}$$

Applying the condition (33) on (32) and (30), and assuming $SI(t) \neq 0$,

$$ES(t) = A_a(t) = SI(t)G_a(t) = u(t) \tag{34}$$

Assuming that g_a and g_a^* represent the weight of network A during and after adjustment, respectively; and $ES'(t) = SI(t)G_a(t)$ and $ES' = SI(t)G_a^*$ denote ES signal before and after adjustment, respectively. The weight adjustment of δg_a is written as follows:

$$\delta g_a(t) = \alpha SI(t)[max(0, (ES(t) - ES'(t))] \tag{35}$$

when $ES(t) - ES' > 0$, (35) decreases to

$$\begin{aligned}\mu g_a(t) &= \alpha SI(t)(ES(t) - ES') \\ &= \alpha SI(t)\left(SI(t)g_a^*(t) - SI(t)G_a(t)\right) \\ &= \alpha SI^2(t)\left(G_a^*(t) - G_a(t)\right) \\ &= \alpha SI^2(t)\tilde{G}_a(t)\end{aligned} \tag{36}$$

where, $\tilde{G}_a(t) = G_a^*(t) - G_a(t)$. In a slight duration of δt, $G_a(t)$ varies as

$$\begin{aligned}G_a(t + \delta t) &= G_a(t) + \delta g_a(t) \\ \tilde{G}_a(t + \delta t) &= G_a^*(t + \delta t) - G_a(t + \delta t) \\ &= G_a^*(t + \delta t) - G_a(t) - \delta g_a(t) \\ &= \tilde{G}_a(t) - \alpha SI^2 \tilde{G}_a(t) \\ &= (1 - \alpha SI^2)\tilde{G}_a(t)\end{aligned} \tag{37}$$

Therefore, $\tilde{G}_a(t + \delta t) \to \tilde{G}_a(t)$ if $|1 - \alpha SI^2| < 1$. The adjustment in Network O is expressed as

$$\begin{aligned}\delta h(t) &= \beta SI(t)(A(t) - O(t) - ES(t)) \\ &= \beta SI(t)\left(0 - SI(t)H(t) - SI(t)G_a^*(t)\right) \\ &= -\beta SI^2(t)\left(G_a^*(t) + H(t)\right) \\ &= -\beta SI^2(t)\tilde{H}(t)\end{aligned} \tag{38}$$

where $\tilde{H}(t) = G_a^*(t) + H(t)$. The term $H(t)$ varies as

$$\begin{aligned}H(t + \delta t) &= H(t) + \delta h(t) \\ \tilde{H}(t + \delta t) &= G_a^*(t + \delta t) + H(t + \delta t) \\ &= G_a^*(t + \delta t) + H(t) + \delta h(t) \\ &= \tilde{H}(t) - \beta S^2 \tilde{H}(t) \\ &= (1 - \beta SI^2)\tilde{H}(t)\end{aligned} \tag{39}$$

Therefore, $\tilde{H}(t + \delta t) \to \tilde{H}(t)$ if $|1 - \beta SI^2| < 1$.

Remark I. *The convergence conditions given in Theorem 1 should be considered when selecting α and β.*

To achieve the promising performance of the BELBIC, forming an empirical relation between SI, ES, and output (u) is crucial. For the BELBIC in the secondary frequency control (represented as BELBIC#1 in Fig. 3), u is the frequency compensator signal ω_{sec}, and for the BELBIC in the secondary voltage control (represented as BELBIC#2 in Fig. 3), u is the voltage compensator signal V_{sec}.

B. Design of SI and ES in BELBIC#1

The SI and ES inputs for BELBIC#1 are selected as (40) and (41) respectively.

$$SI = \phi_1(\omega_{ref}^* - \omega_{MG}) + \phi_2 \int (\omega_{ref}^* - \omega_{MG})dt \tag{40}$$

$$ES = \gamma_1(\omega_{ref}^* - \omega_{MG}) + \gamma_2 \int (\omega_{ref}^* - \omega_{MG})dt + \gamma_3 \omega_{sec} \tag{41}$$

where ϕ_1 and ϕ_2 are weighting coefficients for the SI function; γ_1, γ_2, and γ_3 denote weighting coefficients for the ES function; ω_{ref}^* denotes the average reference frequency of the MG; and ω_{MG} is the frequency average for all DGs, which is expressed as follows:

$$\omega_{MG} = \frac{\sum_{i=1}^{N} \omega_{DG_i}}{N} \tag{42}$$

where N is the number of DGs in the MG.

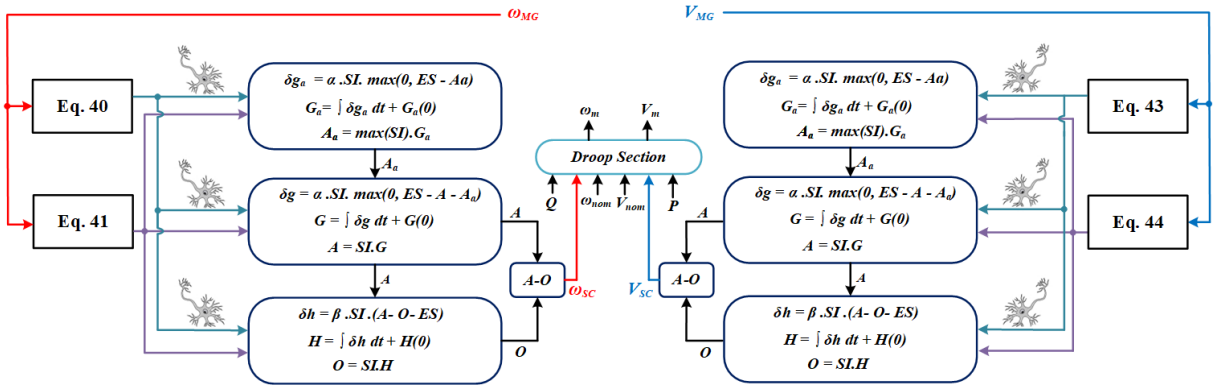

Fig. 4: Block diagram of the proposed secondary control scheme

The values of these weighting coefficients are obtained through a trial and error process. The rationale behind the outlined SI and ES functions is to achieve fast response, a minimum overshoot and steady-state error, and a minimum deviation from an arbitrary reference. The functions SI and ES are, therefore, chosen as the outputs of a PI block in response to $\omega^*_{ref} - \omega_{MG}$.

C. Design of SI and ES in BELBIC#2

Similar to frequency control, the SI and ES inputs for BELBIC#2 can be given as:

$$SI = \phi'_1(v^*_{ref} - v_{MG}) + \phi'_2 \int (v^*_{ref} - v_{MG})dt \tag{43}$$

$$ES = \gamma'_1(v^*_{ref} - v_{MG}) + \gamma'_2 \int (v^*_{ref} - v_{MG})dt + \gamma'_3 v_{sec} \tag{44}$$

where v_{MG} represents the average of voltages broadcasted from each DG. A voltage observer is employed to estimate the average voltage of the MG [40], which is expressed by

$$v_{MG} = \frac{\sum_{i=1}^{N} v_{DG_i}}{N} \tag{45}$$

The weighting coefficients ϕ'_1, ϕ'_2, γ'_1, γ'_2, and γ'_3, as in (40) and (41), are determined through a trial and error process. The trial-and-error procedure was conducted by the knowledge of the designer based on the experience about the SC level and admissible search space of the control signal. The functions SI and ES, as in (40) and (41), are selected as the outputs of a PI block in response to $v^*_{ref} - v_{MG}$.

Fig. 4 displays the BELBIC-based SC scheme. Eqs. (42) and (45) imply that the SC controllers are implemented in a distributed manner. The SC level is settled in each DG as a local controller, while communication links at the upper control level transfer measured data of each unit. SC collects frequency and voltage from other DG units, averages them, and broadcasts their value to the other DGs. The frequency and voltage compensator signals are eventually sent to the droop section to regulate the reference frequency and voltage.

Desirable scaling factors (SFs) are also considered in the output signals of the controllers to attain optimal results. A particle swarm optimization algorithm tunes the SFs by minimizing the following performance index.

$$min\ F = \sum_{i=1}^{N} \left(\int_{t=0}^{T_s} t \left(\Delta\omega_{DGi}{}^2 + \Delta v_{DGi}{}^2 \right) dt \right) \tag{46}$$

Decision variables:

$$SF_{\omega i,min} \leq SF_{\omega i} \leq SF_{\omega i,max} \tag{47}$$

$$SF_{vi,min} \leq SF_{vi} \leq SF_{vi,max} \tag{48}$$

As (46) indicates, the integral of time multiplied by squared error is utilized to get the optimal solution. For each controller, the minimum and maximum values for SFs are considered as 0.1 and 5, respectively.

Remark II. *The common features of this method and the main reasons for its selection are twofold. First, this method has the capability to produce dynamic outputs for control purposes. This includes generating the control commands in the SC loop with respect to the operating point variations and the occurrence of any disturbance as opposed to the conventional controllers. The proposed controller compensates for the steady-state voltage and frequency deviations using an entirely distributed procedure and preserves active and reactive power sharing during both steady state and transitions. Second, this intelligent method has model-free structures and their functionalities are independent of the dynamic model and complexities of the MG. This feature provides a great flexibility in design and facilitates the use of the proposed method in practice. The application of this control method in this paper is based on the supervisory (on-line) regulation application.*

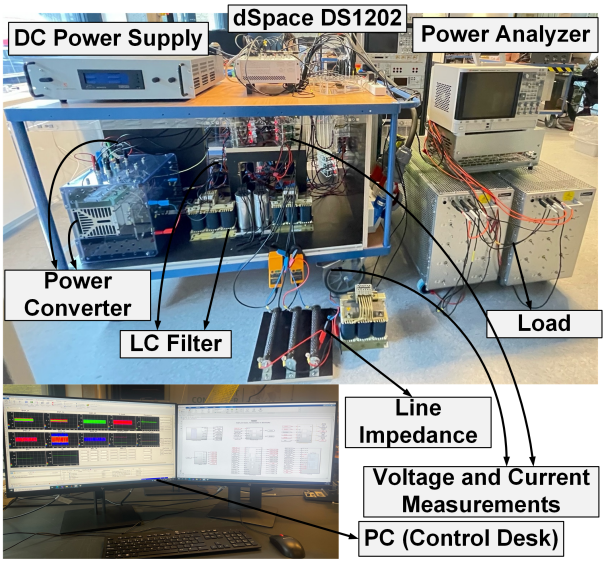

Fig. 5: General view of the experimental setup.

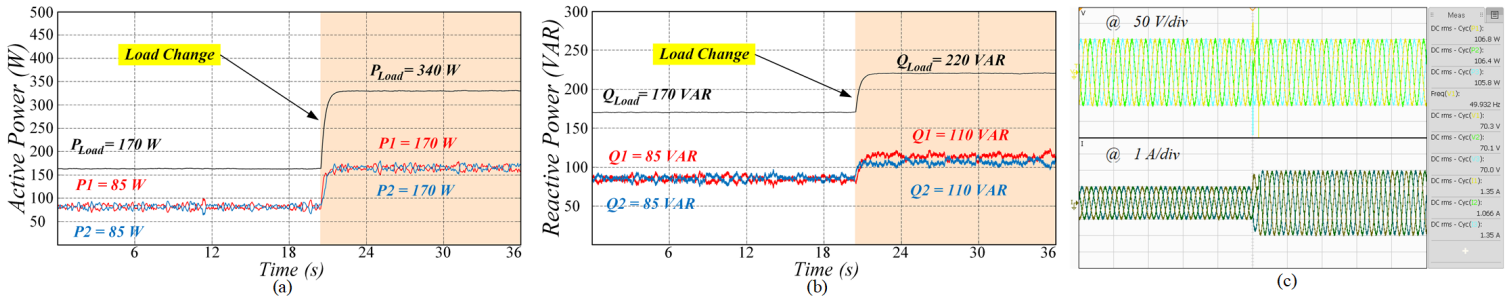

Fig. 6: Experimental results of the transient power-sharing accuracy between two VSCs with equal power-sharing rates for the proposed distributed intelligent secondary control technique. (a), (b), and (c) Active and reactive power, voltage and current diagrams.

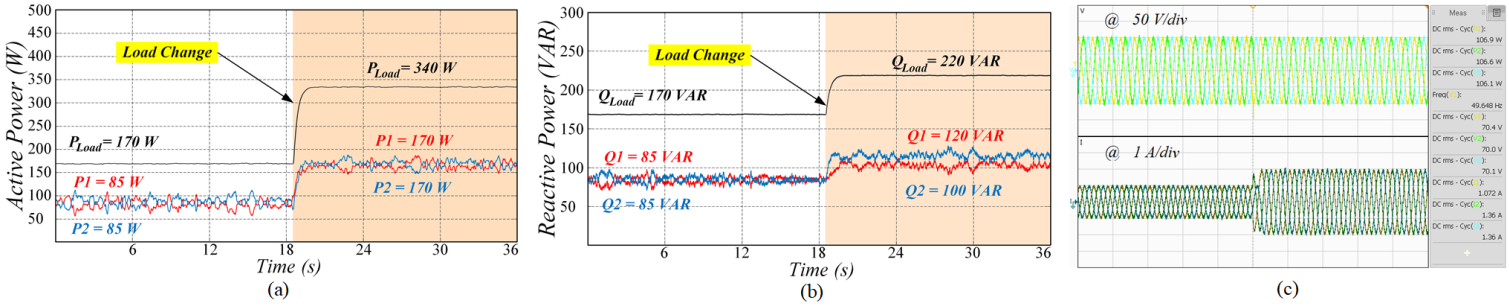

Fig. 7: Experimental results of the transient power-sharing accuracy between two VSCs with equal power-sharing rates for the conventional PI controller. (a), (b), and (c) Active and reactive power, voltage and current diagrams.

IV. Simulation and Experimental Results

In order to verify the proposed distributed intelligent secondary control technique, the simulations have been provided in MATLAB SimPower system, and the experiments have been carried out in a hardware in the loop (HiL) setup includes two DGs with two VSCs, as shown in Fig. 3. The reference voltage and frequency are 100 V and 50 Hz respectively, and the other parameters are demonstrated in Table 1. Five different test cases are investigated to evaluate the performance of the proposed controller. Three of them are provided with experimental results (Case 1 to 3), and the performance of the proposed controller is compared with the conventional PI controller. Two of them are simulated (Case 4 and 5). The obtained results of the proposed controller have analyzed against the ANN-PI, and the conventional PI. These cases are equal and unequal power-sharing rates, unbalanced grid-line impedance, comparative performance analysis among different controllers, and implementing the proposed controller on a MG with three VSCs by considering a communication time delay (disturbance). Fig. 5 demonstrates the utilized components such as measurements, grid-line impedance, loads, power supply, and control unit of the islanded AC MG with details. Two full-bridge three-phase VSCs (SEMITEACH IGBT, 20kW), a DC power supply (Delta Elektronika SM1500-CP-30), eight current and six voltage measurements, two LC filters, two line impedance, and two loads (load 1 is 60 Ω and load 2 is 30 Ω) are utilized in the experimental setup. A dSpace MicroLabBox DS-1202 is employed in the control unit, and a soft driving system, some protection circuits, and a switching algorithm are designed in the practical section. Fig. 5 presents a general view of the existed

TABLE I: Parameters Value of the System

Parameters	Symbol	Value
Output voltage of rectifier	V_{dc}	260 V
Nominal voltage magnitude	v_i	100 V
Nominal frequency	f	50 Hz
Sampling time	T_s	50 μs
Capacitance of LC filter	C_f	$2{\times}5\mu s$
Virtual impedance	Z_v	3.8j Ω
Impedance of LC filter	Z_f	$0.5\Omega + 2.2mH$
Line impedance	Z_l	$0.5\Omega + 2.2mH$
Extra line impedance	$Z_{l,unb}$	$0.5\Omega + 2.2mH$
Load resistance (load 1)	R_{L1}	60 Ω
Load resistance (load 2)	R_{L2}	30 Ω
P - w droop coefficient (DG1 & DG2)	D_P	0.002 rad/W
Q - v droop coefficient (DG1 & DG2)	D_Q	0.01 $V/VAr.s$

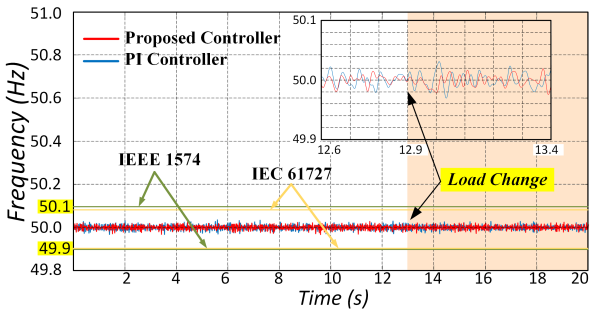

Fig. 8: Experimental results of the transient frequency between two DGs with equal power-sharing rates for the secondary control in both the proposed control technique and the conventional PI controller.

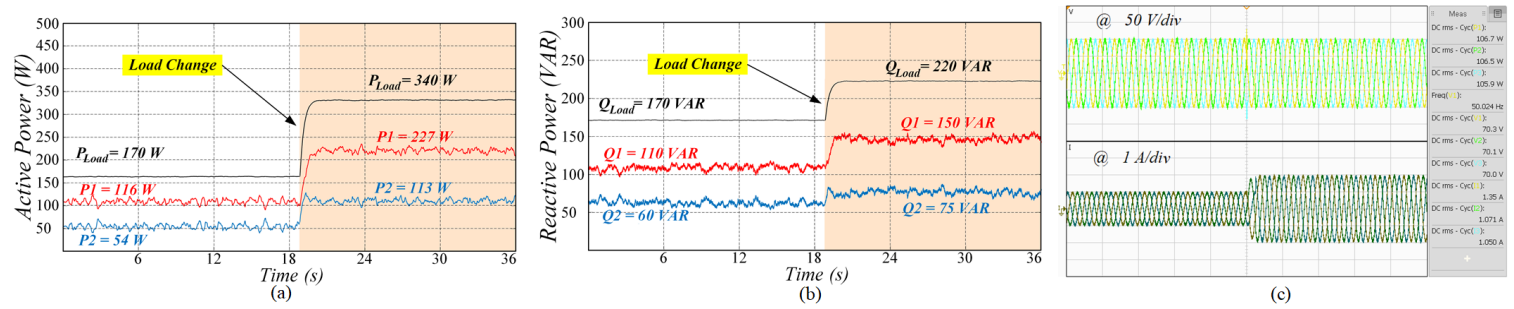

Fig. 9: Experimental results of the transient power-sharing accuracy between two VSCs with unequal power-sharing rates for the proposed distributed intelligent secondary control technique. (a), (b), and (c) Active and reactive power, voltage and current diagrams.

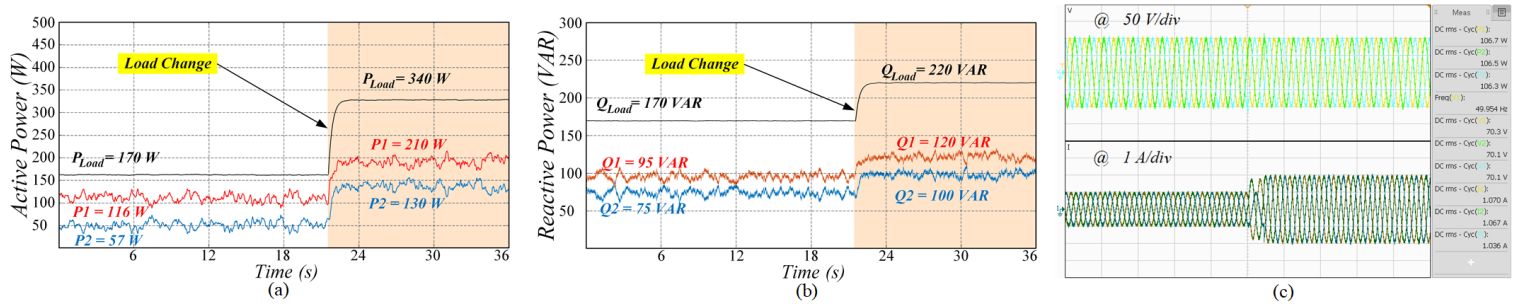

Fig. 10: Experimental results of the transient power-sharing accuracy between two VSCs with unequal power-sharing rates for the conventional PI controller. (a), (b), and (c) Active and reactive power, voltage and current diagrams.

setup in the smart converter lab at DTU, and a view of the Control Desk templates, and related block diagrams in MATLAB/Simulink.

A. Case 1: Equal Power Sharing

In this case study, the performance of the proposed distributed intelligent SC technique is compared with the conventional PI controller. Figs. 6 and 7 present the experimental results of the variations of the active and reactive power for both the control techniques in different load conditions. In this part of the practical results, the PC and SC sections are activated. For the first step, load 1 (R_{L1}) was connected to the system, and then, for the second step, load 2 (R_{L2}) was connected to the setup, and the tests were implemented for both control techniques. Therefore, during the load change, two times more active power is injected into the load through the power converters. By utilizing the FCS-MPC control technique in the PC section, the BW of the voltage control has increased a lot. Therefore, there are no issues between the outer loop and the inner loop connections anymore, and the fluctuations generated by the harmonics in the measured active and reactive power are almost suppressed by the SC section. It's clear, that the proposed intelligent control technique has a fast dynamic response and lower fluctuations than the conventional PI controller in active and reactive power distribution. Besides in Figs. 6 (c) and 7 (c), the experimental results were taken with the power analyzer, which can verify a fast and accurate voltage and current restoration with the proposed controller. In addition, active power, average current and voltage for each phase of the load side, and the system's frequency are also demonstrated. As it can be seen from Fig. 8, the frequency deviations of both controllers are considered the standards IEEE 1574 and IEC 61727. Based on IEEE 1574, 0.8% over frequency and 1% under frequency fluctuations are allowable, and based on IEC 61727, 1% over and under frequency, deviations are allowable in this voltage range [10]. According to Fig. 8, the average frequency deviation of the proposed intelligent controller is around 30% lower than the conventional PI controller.

B. Case 2: Unequal Power Sharing

To validate the results of the proposed control technique, another case test with unequal power-sharing rate of DGs is presented in Figs. 9 and 10. In this case, the power-sharing rates of VSC1 is two times of DG2. It is clear that the proposed control technique can sufficiently share the active and reactive power between two DGs more precisely and faster dynamic performance than the conventional PI controller. Besides, the fluctuation ranges of both active and reactive power for the proposed controller is lower than the conventional PI controller with the same operating condition. Based on Figs. 9 (c) and 10 (c), the current and voltage restoration has a better performance with the proposed controller than the conventional PI controller.

C. Case 3: Unbalanced Grid-Line Impedance

To verify the robustness of the proposed control technique, an uncertainty of the system's parameters is checked out on the grid-line impedance. In this part, an inductance load with a small resistance was added to the grid-line $Z_{l,unb}$ of DG2. By adding the extra impedance to the DG2, the total active power decreases to 330 W. The experimental results present a fast dynamic response, and a perfect tracking reference voltage and frequency for the proposed control technique in comparison with the conventional PI controller. Figs. 11 and 12 present a diagram of the powerful performance of the proposed intelligent SC against the conventional PI controller in equal power-sharing with unbalanced grid-line impedance in the SC section. The proposed intelligent SC is well-designed to adaptive itself with the variations of the load- and line- parameters.

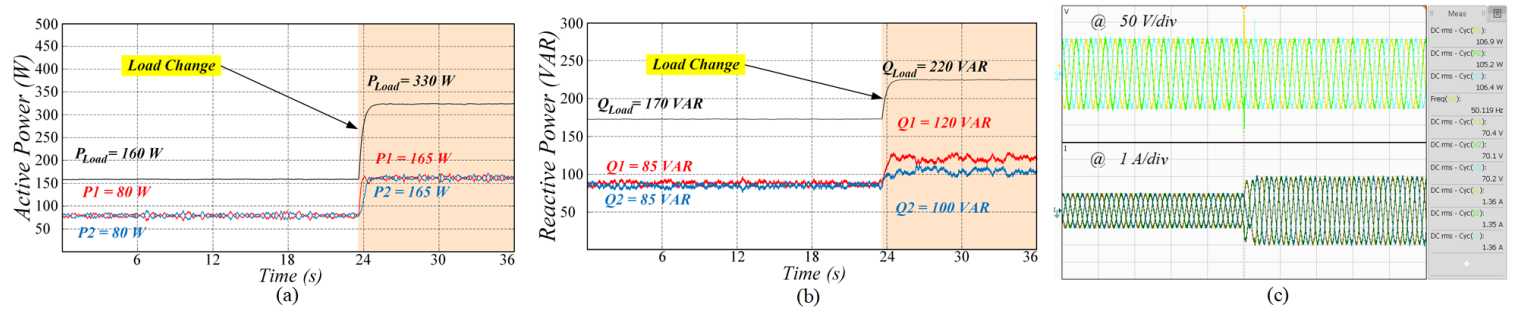

Fig. 11: Experimental results of the transient power-sharing accuracy between two VSCs with unbalanced grid-line impedance for the proposed distributed intelligent secondary control technique. (a), (b), and (c) Active and reactive power, voltage and current diagrams.

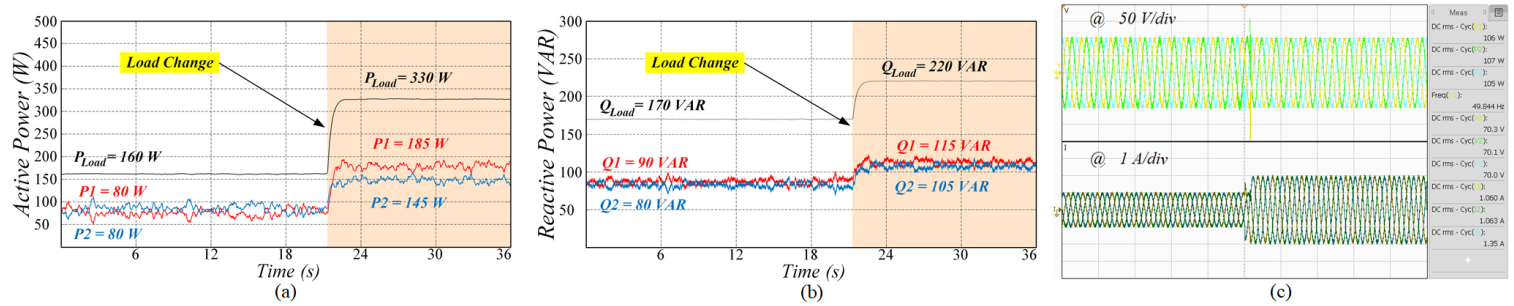

Fig. 12: Experimental results of the transient power-sharing accuracy between two VSCs with unbalanced grid-line impedance for the conventional PI controller. (a), (b), and (c) Active and reactive power, voltage and current diagrams.

In this study, FCS-MPC was utilized as the primary controller, and the conventional PI and the proposed intelligent control techniques are operated in the secondary section. Due to the same primary section and an equal number of measurements (voltage and current), the calculated burden time or sampling time was analyzed in the Control Desk environment for both control techniques, and the lowest value changed from 25 μs to 35 μ. The calculated sampling time shows the capability of the selected control unit and available components of the HiL setup, especially the voltage and current measurements. The prepared setup can easily operate the utilized controllers with a 50 μs sampling time ratio (Table I).

D. Case 4: Comparative Performance Assessment

In this case study, to peruse the performance of the proposed intelligent controller, a comparison has been provided among the ANN-PI [41], the conventional PI, and the proposed technique in the secondary section. The ANN has been employed as a tuner for the PI controller and designs the parameters of K_P and K_I in an online manner. A feed-forward ANN structure with a back-propagation training algorithm is utilized. The structure of ANN includes 2 neurons in the input layer, 20 neurons in the first hidden layer, 7 neurons in the second layer, and 2 neurons in the output layer. Fig. 13 (a) and (b) illustrate the accuracy of dynamic response with two VSCs for each controllers. In this scenario, power-sharing rates are equal. It is obvious that the proposed intelligent controller (BELBIC) has a faster dynamic response on power-sharing accuracy in both active and reactive power in compared with the ANN-PI and the conventional PI.

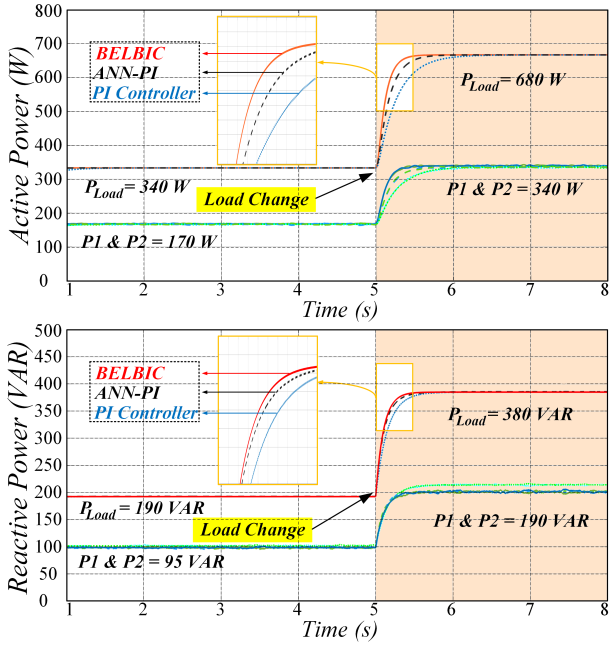

Fig. 13: Simulation results of a comparison of the transient power-sharing accuracy between two VSCs with equal power-sharing rates for the proposed distributed intelligent secondary technique with ANN-PI controller and the conventional PI controller in active and reactive power.

E. Case 5: Equal Power Sharing with Three VSCs

To investigate the performance of the proposed distributed intelligent secondary control technique for more contributed VSCs, a scenario with three VSCs is analyzed with equal power-sharing rates. In this case study, the load changes at t = 4s from 40Ω to 20Ω. Fig. 14 (a) and (b) present the accuracy and the fast dynamic response of active and reactive power-sharing between three VSCs for the proposed control technique. In Fig. 14 (c) and

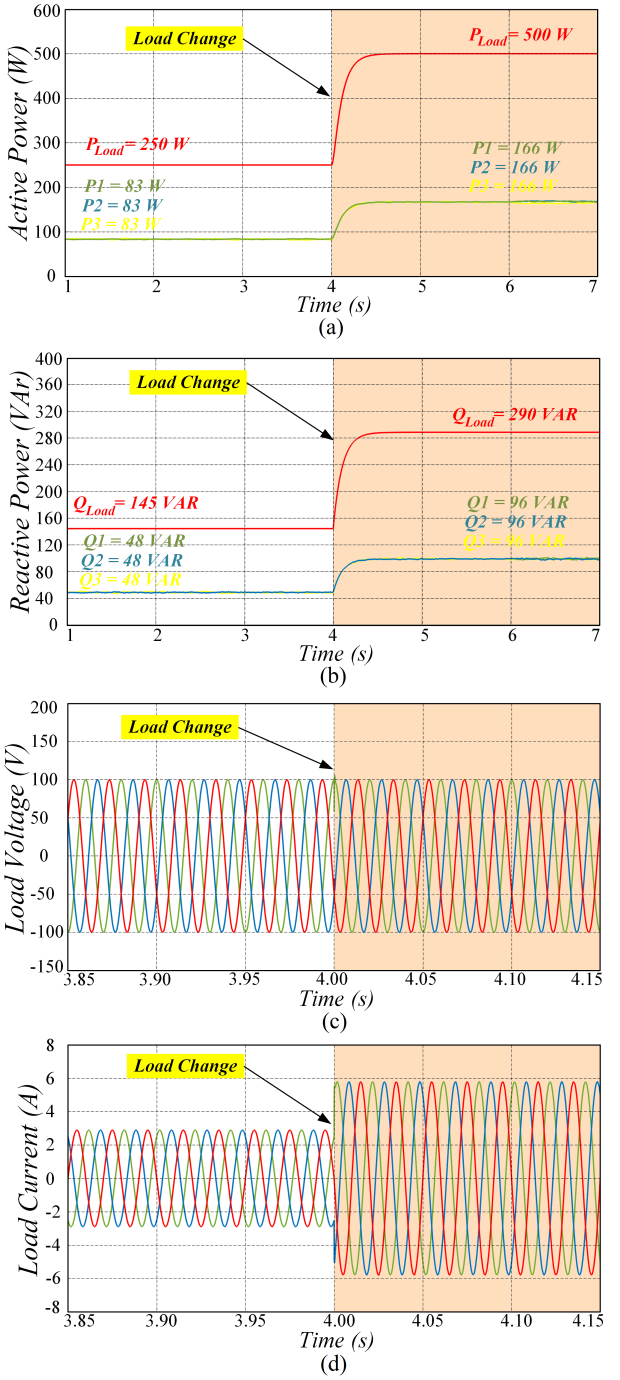

Fig. 14: Simulation results of the transient power-sharing accuracy between three VSCs with equal power-sharing rates for the proposed distributed intelligent secondary control technique. (a), (b), Active and reactive power, (c) and (d) Voltage and current diagrams.

(d), fast dynamic response and restoration are presented for both voltage and current diagrams. Sharing data on a communication link among DGs relies on the control structure of a system. The dynamic response of the proposed controller is much faster than the linear controller [12].

Fig. 15 presents the effect of communication link delay on the frequency regulation with three VSCs for the proposed intelligent secondary control. In this case, the frequency restoration is illustrated with a 30 ms delay on the communication link (the red line presents the normal operation of the proposed frequency control

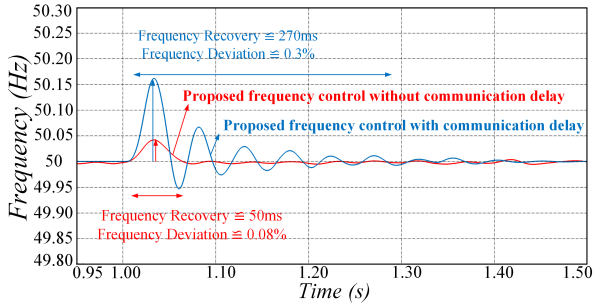

Fig. 15: Frequency restoration with 30 ms communication link delay.

and the blue line shows the proposed frequency control with the communication link delay). The results show that the proposed controller is able to restore the frequency deviation and recovery time with 30 ms delay in the communication link.

V. Conclusion

This paper proposed an intelligent secondary control scheme for VSC-based islanded AC Microgrid. Firstly, an FCS-MPC method is used in the inner level of the PC section to control the voltage of VSCs. The VSCs' voltage regulation is improved with a fast transient response by employing FCS-MPC. Then, the BELBIC is used in the SC loop to recover the voltage and frequency magnitude to their nominal values. The SC level is implemented in a distributed manner so that it is settled in each DG as a local controller. Compared to previous studies, the main contribution of the proposed control scheme is that the SC is thoroughly model-free. The proposed controller's key features are the online learning capacity, minimal computational complexity, and no need for prior knowledge of MG dynamics. Experimental verifications, with two DGs, as an islanded ac MG, are conducted to demonstrate the effectiveness of the proposed control scheme. The results assure that the proposed control scheme regulates voltage amplitude and frequency deviations with superior dynamic performance to conventional control structure while sustaining equal power-sharing among parallel VSCs with no communication network requirement. In future work, to enhance the performance of the BILBIC controller, optimization methods can be employed to adjust weighting coefficients optimally.

References

[1] S. Parhizi, H. Lotfi, A. Khodaei, and S. Bahramirad, "State of the art in research on microgrids: A review," *Ieee Access*, vol. 3, pp. 890–925, 2015.
[2] R. H. Lasseter, "Smart distribution: Coupled microgrids," *Proc. IEEE*, vol. 99, no. 6, pp. 1074–1082, 2011.
[3] H. Han, X. Hou, J. Yang, J. Wu, M. Su, and J. M. Guerrero, "Review of power sharing control strategies for islanding operation of ac microgrids," *IEEE Transactions on Smart Grid*, vol. 7, no. 1, pp. 200–215, 2015.
[4] J. M. Guerrero, J. C. Vasquez, J. Matas, L. G. De Vicuña, and M. Castilla, "Hierarchical control of droop-controlled ac and dc microgridsâa general approach toward standardization," *IEEE Transactions on industrial electronics*, vol. 58, no. 1, pp. 158–172, 2010.
[5] O. Palizban and K. Kauhaniemi, "Hierarchical control structure in microgrids with distributed generation: Island and grid-connected mode," *Renewable and Sustainable Energy Reviews*, vol. 44, pp. 797–813, 2015.
[6] M. Ghazzali, M. Haloua, and F. Giri, "Modeling and adaptive control and power sharing in islanded ac microgrids," *International Journal of Control, Automation and Systems*, vol. 18, no. 5, pp. 1229–1241, 2020.
[7] A. Vijay and S. Doolla, "Performance of droop control techniques under nonlinear loading conditions: Uniform and nonuniform configurations," *IEEE Systems Journal*, vol. 15, no. 2, pp. 2245–2256, 2020.

[8] H. Bevrani and S. Shokoohi, "An intelligent droop control for simultaneous voltage and frequency regulation in islanded microgrids," *IEEE transactions on smart grid*, vol. 4, no. 3, pp. 1505–1513, 2013.

[9] Y. Khayat, Q. Shafiee, R. Heydari, M. Naderi, T. Dragičević, J. W. Simpson-Porco, F. Dörfler, M. Fathi, F. Blaabjerg, J. M. Guerrero *et al.*, "On the secondary control architectures of ac microgrids: An overview," *IEEE Transactions on Power Electronics*, vol. 35, no. 6, pp. 6482–6500, 2019.

[10] R. Heydari, Y. Khayat, A. Amiri, T. Dragicevic, Q. Shafiee, P. Popovski, and F. Blaabjerg, "Robust high-rate secondary control of microgrids with mitigation of communication impairments," *IEEE Transactions on Power Electronics*, vol. 35, no. 11, pp. 12 486–12 496, 2020.

[11] S. Shokoohi, S. Golshannavaz, R. Khezri, and H. Bevrani, "Intelligent secondary control in smart microgrids: an on-line approach for islanded operations," *Optimization and Engineering*, vol. 19, no. 4, pp. 917–936, 2018.

[12] R. Heydari, T. Dragicevic, and F. Blaabjerg, "High-bandwidth secondary voltage and frequency control of vsc-based ac microgrid," *IEEE Transactions on Power Electronics*, vol. 34, no. 11, pp. 11 320–11 331, 2019.

[13] T. Dragičević, "Model predictive control of power converters for robust and fast operation of ac microgrids," *IEEE Transactions on Power Electronics*, vol. 33, no. 7, pp. 6304–6317, 2017.

[14] Y. Zhang, A. Mohammadpour Shotorbani, L. Wang, and B. Mohammadi-Ivatloo, "Enhanced pi control and adaptive gain tuning schemes for distributed secondary control of an islanded microgrid," *IET Renewable Power Generation*, vol. 15, no. 4, pp. 854–864, 2021.

[15] S. Ullah, L. Khan, I. Sami, and N. Ullah, "Consensus-based delay-tolerant distributed secondary control strategy for droop controlled ac microgrids," *IEEE Access*, vol. 9, pp. 6033–6049, 2021.

[16] T. Dragičević and M. Novak, "Weighting factor design in model predictive control of power electronic converters: An artificial neural network approach," *IEEE Transactions on Industrial Electronics*, vol. 66, no. 11, pp. 8870–8880, 2018.

[17] R. Heydari, M. Gheisarnejad, M. H. Khooban, T. Dragicevic, and F. Blaabjerg, "Robust and fast voltage-source-converter (vsc) control for naval shipboard microgrids," *IEEE Transactions on Power Electronics*, vol. 34, no. 9, pp. 8299–8303, 2019.

[18] Y. Khayat, R. Heydari, M. Naderi, T. Dragicevic, Q. Shafiee, M. Fathi, H. Bevrani, and F. Blaabjerg, "Decentralized frequency control of ac microgrids: an estimation-based consensus approach," *IEEE Journal of Emerging and Selected Topics in Power Electronics*, vol. 9, no. 5, pp. 5183–5191, 2020.

[19] B. Liu, "System deployment and decentralized control of islanded ac microgrids without communication facility," *Journal of Modern Power Systems and Clean Energy*, vol. 7, no. 4, pp. 913–922, 2019.

[20] Z. Karami, Q. Shafiee, Y. Khayat, M. Yaribeygi, T. Dragičević, and H. Bevrani, "Decentralized model predictive control of dc microgrids with constant power load," *IEEE Journal of Emerging and Selected Topics in Power Electronics*, vol. 9, no. 1, pp. 451–460, 2019.

[21] Y. Khayat, M. Naderi, Q. Shafiee, Y. Batmani, M. Fathi, J. M. Guerrero, and H. Bevrani, "Decentralized optimal frequency control in autonomous microgrids," *IEEE Transactions on Power Systems*, vol. 34, no. 3, pp. 2345–2353, 2018.

[22] X. Hou, Y. Sun, J. Lu, X. Zhang, L. H. Koh, M. Su, and J. M. Guerrero, "Distributed hierarchical control of ac microgrid operating in grid-connected, islanded and their transition modes," *Ieee Access*, vol. 6, pp. 77 388–77 401, 2018.

[23] Z. Li, Z. Cheng, J. Liang, J. Si, L. Dong, and S. Li, "Distributed event-triggered secondary control for economic dispatch and frequency restoration control of droop-controlled ac microgrids," *IEEE Transactions on Sustainable Energy*, vol. 11, no. 3, pp. 1938–1950, 2019.

[24] A. Navas-Fonseca, C. Burgos-Mellado, J. S. Gómez, F. Donoso, L. Tarisciotti, D. Saez, R. Cardenas, and M. Sumner, "Distributed predictive secondary control for imbalance sharing in ac microgrids," *IEEE Transactions on Smart Grid*, vol. 13, no. 1, pp. 20–37, 2021.

[25] A. M. Shotorbani, B. Mohammadi-Ivatloo, L. Wang, S. Ghassem-Zadeh, and S. H. Hosseini, "Distributed secondary control of battery energy storage systems in a stand-alone microgrid," *IET Generation, Transmission & Distribution*, vol. 12, no. 17, pp. 3944–3953, 2018.

[26] A. Bidram, A. Davoudi, F. L. Lewis, and J. M. Guerrero, "Distributed cooperative secondary control of microgrids using feedback linearization," *IEEE transactions on power systems*, vol. 28, no. 3, pp. 3462–3470, 2013.

[27] J. W. Simpson-Porco, Q. Shafiee, F. Dörfler, J. C. Vasquez, J. M. Guerrero, and F. Bullo, "Secondary frequency and voltage control of islanded microgrids via distributed averaging," *IEEE Transactions on Industrial Electronics*, vol. 62, no. 11, pp. 7025–7038, 2015.

[28] Y. Zhang, A. M. Shotorbani, L. Wang, and B. Mohammadi-Ivatloo, "Distributed secondary control of a microgrid with a generalized pi finite-time controller," *IEEE Open Access Journal of Power and Energy*, vol. 8, pp. 57–67, 2021.

[29] Y. Shan, J. Hu, K. W. Chan, and S. Islam, "A unified model predictive voltage and current control for microgrids with distributed fuzzy cooperative secondary control," *IEEE Transactions on Industrial Informatics*, vol. 17, no. 12, pp. 8024–8034, 2021.

[30] Y. Xu, H. Sun, W. Gu, Y. Xu, and Z. Li, "Optimal distributed control for secondary frequency and voltage regulation in an islanded microgrid," *IEEE Transactions on Industrial Informatics*, vol. 15, no. 1, pp. 225–235, 2018.

[31] A. M. Shotorbani, S. Ghassem-Zadeh, B. Mohammadi-Ivatloo, and S. H. Hosseini, "A distributed secondary scheme with terminal sliding mode controller for energy storages in an islanded microgrid," *International Journal of Electrical Power & Energy Systems*, vol. 93, pp. 352–364, 2017.

[32] A. M. Shotorbani, S. G. Zadeh, B. Mohammadi-Ivatloo, and S. H. Hosseini, "A distributed non-lipschitz control framework for self-organizing microgrids with uncooperative and renewable generations," *International Journal of Electrical Power & Energy Systems*, vol. 90, pp. 267–279, 2017.

[33] N. Sarrafan, M.-A. Rostami, J. Zarei, R. Razavi-Far, M. Saif, and T. Dragičević, "Improved distributed prescribed finite-time secondary control of inverter-based microgrids: Design and real-time implementation," *IEEE Transactions on Industrial Electronics*, vol. 68, no. 11, pp. 11 135–11 145, 2020.

[34] M. A. Sharbafi, C. Lucas, and R. Daneshvar, "Motion control of omni-directional three-wheel robots by brain-emotional-learning-based intelligent controller," *IEEE Transactions on Systems, Man, and Cybernetics, Part C (Applications and Reviews)*, vol. 40, no. 6, pp. 630–638, 2010.

[35] B. Debnath and S. Mija, "Emotional learning based controller for quadruple tank systemâan improved stimuli design for multiple set-point tracking," *IEEE Transactions on Industrial Electronics*, vol. 68, no. 11, pp. 11 296–11 308, 2020.

[36] D. C. Marques, J. L. Silva, M. M. S. Lira, and R. R. Aquino, "An emotional discrete controller pso tuned and designed for a real industrial pumping system," *Scientific Reports*, vol. 12, no. 1, pp. 1–24, 2022.

[37] M. U. Saeed, Z. Sun, and S. Elias, "Semi-active vibration control of building structure by self tuned brain emotional learning based intelligent controller," *Journal of Building Engineering*, vol. 46, p. 103664, 2022.

[38] M. Qutubuddin and N. Yadaiah, "Modeling and implementation of brain emotional controller for permanent magnet synchronous motor drive," *Engineering Applications of Artificial Intelligence*, vol. 60, pp. 193–203, 2017.

[39] R. Khezri, A. Oshnoei, A. Yazdani, and A. Mahmoudi, "Intelligent coordinators for automatic voltage regulator and power system stabiliser in a multi-machine power system," *IET Generation, Transmission & Distribution*, vol. 14, no. 23, pp. 5480–5490, 2020.

[40] Y. Zhang, A. M. Shotorbani, L. Wang, and W. Li, "Distributed voltage regulation and automatic power sharing in multi-terminal hvdc grids," *IEEE Transactions on Power Systems*, vol. 35, no. 5, pp. 3739–3752, 2020.

[41] H. Sorouri, M. Sedighizadeh, A. Oshnoei, and R. Khezri, "An intelligent adaptive control of dc–dc power buck converters," *International Journal of Electrical Power & Energy Systems*, vol. 141, p. 108099, 2022.

Mohammad Sadegh Orfi Yeganeh received the B.Sc. degree from Bu-Ali Sina University, Hamadan, Iran, in 2014 and the M.Sc. degree from Imam Khomeini International University, Qazvin, Iran, in 2016, both in electrical engineering. He was also a guest researcher for a year from 2019 at the Department of Energy, Aalborg University, Denmark. He is currently working toward a Ph.D. degree at the DTU Wind and Energy Systems, Technical University of Denmark. His research interests are mainly in power electronics, advanced control techniques on power converters/motor drives, artificial intelligence, and reliability in power electronic applications.

Arman Oshnoei received the M.S. degree in electrical engineering from University of Tabriz, Tabriz, Iran, in 2017, and the Ph.D. degree in Electrical Engineering at Shahid Beheshti University, Tehran, Iran, in 2021. From November 2020 to May 2021, he was a Visiting Ph.D. Scholar with the Department of Energy, Aalborg University, Aalborg, Denmark. From August 2021 to March 2022, he was a research assistant with the Department of Energy, Aalborg University, Aalborg, Denmark, where he is currently a Postdoctoral Researcher. His research interests include modeling and control of power electronic based power systems, power system stability and control, and intelligent control. Dr. Oshnoei has been selected and awarded by the National Elite Foundation of Iran in 2019.

Nenad Mijatovic after obtaining his Dipl.Ing. education in Electrical Power Engineering at University of Belgrade, Serbia in 2007, was enrolled as a doctoral candidate at Technical University of Denmark. He received his Ph.D. degree from Technical University of Denmark for his work on technical feasibility of novel machines and drives for wind industry. Upon completion of his PhD, he continued work within the field of wind turbine directdrive concepts as an Industrial Post-Doc. Dr. N. Mijatovic currently holds position of Associate Professor at Technical University of Denmark where he is in charge of managing research projects and education related to the field of electrical machines and drives, power electronic convertors, motion control, application of energy storage and general applications of low frequency electromagnetism and large-scale application of superconductivity with main focus on emerging eMobility and renewable energy generation.

He is a member of IEEE since 2008 and senior member of IEEE since 2018 and his field of interest and research includes novel electrical machine drives/actuator designs, operation, control and diagnostic of electromagnetic assemblies, advance control of drives and grid connected power electronics, energy storage and eMobility.

Tomislav Dragicevic (S'09-M'13-SM'17) received the M.Sc. and the industrial Ph.D. degrees in electrical engineering from the Faculty of Electrical Engineering, University of Zagreb, Zagreb, Croatia, in 2009 and 2013, respectively. From 2013 until 2016, he was a Postdoctoral Researcher with Aalborg University, Denmark. From 2016 to 2020, he was an Associate Professor with Aalborg University, Denmark. Since 2020, he has been a Professor with the Technical University of Denmark, Lyngby, Denmark. He was a Guest Professor with Nottingham University, U.K., during spring/summer of 2018. He has authored and coauthored more than 250 technical publications (more than 120 of them are published in international journals, mostly in IEEE), 8 book chapters, and a book in the field. His research interests include application of advanced control, optimization, and artificial intelligence-inspired techniques to provide innovative and effective solutions to emerging challenges in design, control, and cyber-security of power electronics-intensive electrical distributions systems and microgrids.

Dr. Dragicevic is an Associate Editor for the IEEE Transactions on Industrial Electronics, IEEE Transactions on Power Electronics, IEEE Emerging and Selected Topics in Power Electronics, and IEEE Industrial Electronics Magazine. He is a recipient of the KonÄar Prize for the best industrial Ph.D. thesis in Croatia, a Robert Mayer Energy Conservation Award, and a winner of an Alexander von Humboldt Fellowship for experienced researchers.

Frede Blaabjerg (S'86-M'88-SM'97-F'03) received the Ph.D. degree in electrical engineering from Aalborg University in 1995. He was with ABB-Scandia, Randers, Denmark, from 1987 to 1988. He became an Assistant Professor, an Associate Professor, and a Full Professor of Power Electronics and Drives with Aalborg University, in 1992, 1996, and 1998, respectively. In 2017, he became a Villum Investigator. He is honoris causa with University Politehnica Timisoara (UPT), Romania, and Tallinn Technical University, Estonia. He has published more than 600 journal papers in the fields of power electronics and its applications. He has coauthored four monographs and an Editor of ten books in power electronics and its applications. His current research interests include power electronics and its applications, such as in wind turbines, PV systems, reliability, harmonics, and adjustable speed drives.

Dr. Blaabjerg has received 33 IEEE Prize Paper Awards, the IEEE PELS Distinguished Service Award in 2009, the EPE-PEMC Council Award in 2010, the IEEE William E. Newell Power Electronics Award 2014, the Villum Kann Rasmussen Research Award 2014, the Global Energy Prize in 2019, and the 2020 IEEE Edison Medal. He was the Editor-in-Chief of the IEEE TRANSACTIONS ON POWER ELECTRONICS from 2006 to 2012. He has been a Distinguished Lecturer for the IEEE Power Electronics Society from 2005 to 2007 and for the IEEE Industry Applications Society from 2010 to 2011 as well as 2017 to 2018. From 2019 to 2020, he served as a President of IEEE Power Electronics Society. He has been a Vice-President of the Danish Academy of Technical Sciences. From 2014 to 2020, he is nominated by Thomson Reuters to be between the most 250 cited researchers in Engineering in the world.